Available online at www.sciencedirect.com
ScienceDirect
Ceramics International 35 (2009) 3135–3141
CERAMICS INTERNATIONAL
www.elsevier.com/locate/ceramint

Variation of cathode properties of $LiNi_{0.975}M_{0.025}O_2$ (M = Ga, In and Tl) prepared by the combustion method

MyoungYoup Song [a,*], SungNam Kwon [b], HyeRyoung Park [c]

[a] Division of Advanced Materials Engineering, Department of Hydrogen and Fuel Cells, Research Center of Advanced Materials Development, Engineering Research Institute, Chonbuk National University, Jeonju, 561-756, Republic of Korea
[b] Department of Hydrogen and Fuel Cells, Chonbuk National University, Jeonju, 561-756, Republic of Korea
[c] Faculty of Applied Chemical Engineering, Chonnam National University, 300 Yongbongdong Bukgu Gwangju, 500-757, Republic of Korea

Received 24 February 2009; received in revised form 18 March 2009; accepted 29 April 2009
Available online 6 June 2009

Abstract

$LiNi_{0.975}M_{0.025}O_2$ (M = Ga, In and Tl) were synthesized by the combustion method (by preheating at 400 °C for 30 min in air and then calcining in an O_2 stream at 750 °C for 36 h). XRD analyses, SEM observation and measurement of the variation of discharge capacity with the number of cycles were carried out. All the samples had the $R\bar{3}m$ structure, and $LiNi_{0.975}In_{0.025}O_2$ contained $LiInO_2$ phase as an impurity. Among these samples, $LaNi_{0.975}Ga_{0.025}O_2$ had the largest first discharge capacity (172.2 mAh g^{-1}) and relatively good cycling performance (discharge capacity 140.3 mAh g^{-1} at $n = 20$). For $LiNi_{0.975}M_{0.025}O_2$ (M = Ga, In and Tl), the first discharge capacity decreased with increase in the ionic radius of the substituted element. The variation of cation mixing with the substituted element (decrease in $I_{0\,0\,3}/I_{1\,0\,4}$ and increase in *R*-factor from M = Ga through M = Tl) is considered to be related to the behavior of the first discharge capacity with the substituted element.

Keywords: $LiNi_{0.975}M_{0.025}O_2$ (M = Ga; In and Tl); Substituted ion radius; Combustion method; $I_{0\,0\,3}/I_{1\,0\,4}$; *R*-factor; Cation mixing

1. Introduction

The transition metal oxides such as $LiMn_2O_4$ [1–3], $LiCoO_2$ [4–6] and $LiNiO_2$ [7–14] have been investigated as cathode materials for lithium secondary batteries. $LiMn_2O_4$ is relatively cheap and does not bring about environmental pollution, but its cycling performance is not good. $LiCoO_2$ has a large diffusivity and a high operating voltage, and it can be easily prepared. However, it has a disadvantage that it contains an expensive element Co. $LiNiO_2$ is a very promising cathode material since it has a large discharge capacity [15] and is relatively excellent from the viewpoints of economics and environment. However, its preparation is very difficult as compared with $LiCoO_2$ and $LiMn_2O_4$.

It is known that $Li_{1-x}Ni_{1+x}O_2$ forms rather than stoichiometric $LiNiO_2$ during preparation. This phenomenon is called cation mixing (disordering). Excess nickel occupies the Li sites, destroying the ideally layered structure and preventing lithium ions from easy movement for intercalation and de-intercalation during cycling. This results in a small discharge capacity and a poor cycling performance.

To improve the electrochemical properties of $LiNiO_2$, Co^{3+}, Al^{3+}, Mn^{3+}, $Ga^{3+}$and Ti^{4+} ions were substituted for lithium ion [16–29]. Rougier et al. [19] reported that the stabilization of the two-dimensional character of the structure by cobalt substitution in $LiNiO_2$ is correlated with an increase in the cell performance due to the decrease in the amount of extra nickel ions in the inter-slab space which impede the lithium diffusion. Guilmard et al. [24] investigated the electrochemical performances of $LiNi_{1-y}Al_yO_2$ ($0.10 \leq y \leq 0.50$) synthesized by a co-precipitation method, and showed that aluminum substitution suppressed all the phase transitions observed for the $LiNiO_2$ system. Guilmard et al. [25] reported the presence of 5% or 3% extra nickel ions in the inter-slab space, respectively, in two types of $LiNi_{0.90}Mn_{0.10}O_2$ synthesized by a co-precipitation method in the presence of either 5 or 50%

* Corresponding author. Tel.: +82 63 270 2379; fax: +82 63 270 2386.
E-mail address: songmy@chonbuk.ac.kr (M. Song).

0272-8842/$36.00
doi:10.1016/j.ceramint.2009.04.025

lithium excess. Cycling test showed a decrease in the electrochemical properties with a large irreversible capacity at the end of the first cycle, in comparison with $LiNiO_2$. Nishida et al. [15] investigated gallium-doping to $LiNiO_2$. They found that it was effective to improve the cycling behavior of $LiNiO_2$. The obtained specimen was single phase with hexagonal structure. The crystal structure during charging process was stabilized by gallium doping. Hexagonal structure was retained all over the charging state without monoclinic phase and without two hexagonal phase regions which are observed in undoped $LiNiO_2$. The gallium-doped $LiNiO_2$ showed superior rechargeable capacity of 190 mAh g^{-1} and retention of more than 95% after 100 cycles in the cycling test between 3.0 and 4.3 V at room temperature. Chang et al. [20] detected partial disordering between transition metal (Ni and Ti) layer and lithium by the Rietveld refinement in $Li_xNi_{1-y}Ti_yO_2$ ($0.1 \leq y \leq 0.5$) prepared by solid state reaction. By considering the ionic radius and the Ni–O bond length, the Ni(II) ions are concluded to be partially stabilized in the lithium site. According to Gao et al. [17] and Kim and Amine [22,23], the substitution of Ti for Ni resulted in a large discharge capacity and a good cycling performance.

Tong et al. [30] synthesized and characterized $LiCo_{0.3-x}Ga_xNi_{0.7}O_2$ ($x = 0$, 0.05) as a cathode material. The single phase of $LiCo_{0.3-x}Ga_xNi_{0.7}O_2$ ($x = 0, 0.05$) was synthesized by a sol–gel method. The synthesized $LiCo_{0.25}Ga_{0.05}Ni_{0.7}O_2$ exhibited better electrochemical performance with an initial discharge capacity of 180.0 mAh g^{-1} and a capacity retention of 95.2% after 50 cycles between 2.8 and 4.4 V at 0.2 C rate. The study on the structural evolution of the material during the cycling showed that Ga-doping improved the structure stability of $LiCo_{0.3}Ni_{0.7}O_2$ at ambient temperature and 55 °C. Furthermore, thermal stability of the charged $LiCo_{0.25}Ga_{0.05}Ni_{0.7}O_2$ was improved.

$LiNiO_2$ synthesized by the solid-state reaction method does not have large discharge capacity and does not exhibit good cycling performance, probably because it has poor crystallinity and non-homogeneous particle size. On the other hand, homogeneous mixing of starting materials is possible by the combustion method because nitrates as starting materials and urea as a fuel are mixed in distilled water by a magnetic stirrer. This may lead to good crystallinity and homogeneous particle size when the sample is synthesized.

Combustion synthesis is based on the field of propellants and explosives. Combustion synthesis is a chemical reaction between the metal salts and suitable organic fuel. The reaction accompanies an exothermic and self-sustaining chemical reaction [31]. Its processing feature is that the initial heat is required for starting the chemical reaction. Afterward, the chemical reaction supplies the energy to react the materials itself without external energy [32].

In this work, Ni in $LiNiO_2$ was substituted by Ga, In and Tl with different ionic radii. The ionic radii of Ga, In and Tl are 0.62, 0.79 and 0.88 Å, respectively. $LiNi_{0.975}M_{0.025}O_2$ (M = Ga, In and Tl) samples were synthesized by the combustion method. The electrochemical properties of the synthesized samples were then investigated.

2. Experimental

The optimum conditions to synthesize $LiNiO_2$ by the combustion method, studied in our previous work [33], were preheating at 400 °C for 30 min in air and then calcining at 750 °C for 36 h in an O_2 stream. $LiNi_{0.975}M_{0.025}O_2$ (M = Ga, In and Tl) were synthesized under these conditions. Lithium nitrate ($LiNO_3$, Aldrich Chemical), nickel hexahydrate ($Ni(NO_3)_2{\cdot}6H_2O$, Aldrich Chemical), $GaNO_3{\cdot}xH_2O$ (Aldrich Chemical, 99.999%) or $In(NO_3)_3{\cdot}5H_2O$ (Aldrich Chemical, 99.99%) or $TlNO_3$ (Aldrich Chemical, 99.9%) were used as starting materials. The starting materials, in the desired proportions, were mixed with urea homogeneously by a magnetic stirrer. The mole ratio of urea to nitrate was 3.6. The heating rate was about 100 °C h^{-1} and the cooling rate was about 100 °C h^{-1}.

The phase identification of the synthesized samples was carried out by X-ray diffraction analysis using CuK_α radiation. A Rigaku III/A X-ray diffractometer was used. The scanning rate was 6° min^{-1} and the scanning range of diffraction angle (2θ) was $10° \leq 2\theta \leq 80°$. The morphologies of the samples were observed by scanning electron microscopy (SEM).

To measure the electrochemical properties, the electrochemical cells consisted of the prepared sample as a positive electrode, Li metal as a negative electrode and an electrolyte of 1 M $LiPF_6$ in a 1:1 (volume ratio) mixture of ethylene carbonate (EC) and diethyl carbonate (DEC). A Whatman glass fiber was used as a separator. The cells were assembled in an argon-filled dry box. To fabricate the positive electrode, active material, acetylene black and polyvinylidene fluoride (PVDF) binder with *N*-methyl-2-pyrrolidone (NMP) were mixed in a weight ratio 85:10:5 on Al foil. All the electrochemical tests were performed at room temperature with a battery charge–discharge cycle tester at 0.1 C rate in a potential range from 2.7 to 4.4 V.

Fig. 1 shows experimental procedure for the preparation by the combustion method and the characterization of $LiNi_{0.975}M_{0.025}O_2$ (M = Ga, In and Tl) cathodes.

3. Results and discussion

Fig. 2 shows X-ray powder diffraction (XRD) patterns of $LiNi_{0.975}M_{0.025}O_2$ (M = Ga, In and Tl) samples calcined at 750 °C for 36 h. All the samples have the peaks for the phase with the α-$NaFeO_2$ structure of the rhombohedral system (space group; $R\bar{3}m$). The $LiNi_{0.975}In_{0.025}O_2$ sample has the peaks for $LiInO_2$ in addition to those for the phase with the α-$NaFeO_2$ structure. The $R\bar{3}m$ structure is distorted in the *c*-axis direction of the hexagonal structure. This is reflected by the split of the 0 0 6 and 1 0 2 peaks, and of the 1 0 8 and 1 1 0 peaks in the XRD patterns. The 0 0 6 and 1 0 2 peaks were not split, but the 1 0 8 and 1 1 0 peaks were split for all the samples.

Ohzuku et al. [34] reported that, the electrochemically reactive $LiNiO_2$ showed larger integrated intensity ratio of 0 0 3 peak to 1 0 4 peak ($I_{0\,0\,3}/I_{1\,0\,4}$) and a clear split of the 1 0 8 and 1 1 0 peaks in their XRD patterns. The degree of cation mixing (displacement of nickel and lithium ions) is low if the value of $I_{0\,0\,3}/I_{1\,0\,4}$ is large and the 1 0 8 and 1 1 0 peaks are split clearly. The value of $(I_{0\,0\,6} + I_{1\,0\,2})/I_{1\,0\,1}$, called the *R*-factor, is known to

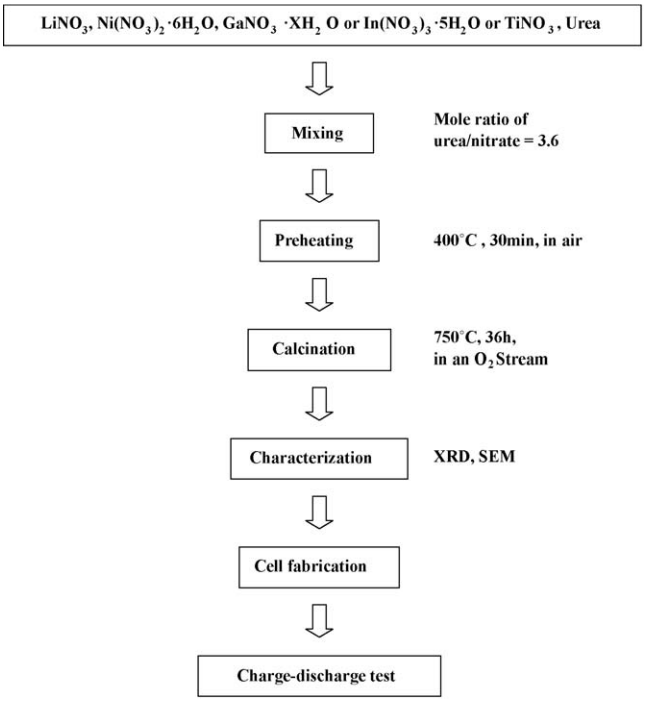

Fig. 1. Experimental procedure for the preparation by the combustion method and the characterization of $LiNi_{0.975}M_{0.025}O_2$ (M = Ga, In and Tl) cathodes.

be smaller as the unit cell volume of $Li_yNi_{2-y}O_2$ gets smaller. The *R*-factor increases as y in $Li_yNi_{2-y}O_2$ decreases for *y* near 1. This indicates that the *R*-factor increases as the degree of cation mixing becomes larger [7]. The cation mixing in layered materials makes sliding between basal planes impossible, resulting in the electrochemical inactivity of the materials [34].

Table 1 gives lattice parameters *a* and *c*, *c*/*a*, $I_{0\,0\,3}/I_{1\,0\,4}$, *R*-factor and unit cell volume calculated from XRD patterns of $LiNi_{0.975}M_{0.025}O_2$ (M = Ga, In and Tl) calcined at 750 °C for 36 h. The $LiNi_{0.975}Ga_{0.025}O_2$ sample has the largest $I_{0\,0\,3}/I_{1\,0\,4}$ and the smallest value of *R*-factor.

Fig. 3 shows the SEM photographs of $LiNi_{0.975}M_{0.025}O_2$ (M = Ga, In and Tl) calcined at 750 °C for 36 h. The samples contain agglomerated particles and relatively small particles on the agglomerates. The particles on the agglomerates

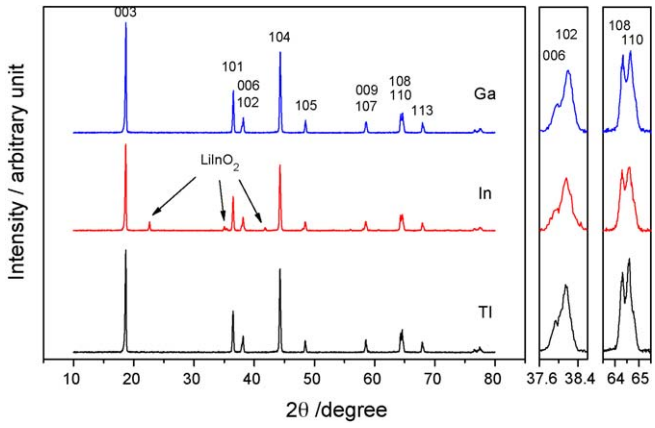

Fig. 2. XRD patterns of $LiNi_{0.975}M_{0.025}O_2$ (M = Ga, In and Tl) calcined at 750 °C for 36 h.

Table 1
Data calculated from XRD patterns of $LiNi_{0.975}M_{0.025}O_2$ (M = Ga, In and Tl) calcined at 750 °C for 36 h.

M	*a* (Å)	*c* (Å)	*c*/*a*	$I_{0\,0\,3}/I_{1\,0\,4}$	*R*-factor	Unit cell volume (Å^3)
Ga	2.881	14.218	4.935	1.366	0.509	102.209
In	2.880	14.377	4.992	1.317	0.531	103.284
Tl	2.881	14.213	4.933	1.229	0.647	102.187

of $LiNi_{0.975}Ga_{0.025}O_2$ are in the form of polyhedron with flat surfaces. The particles on the agglomerates of $LiNi_{0.975}In_{0.025}O_2$ have flat or undulated surfaces. The particles on the agglomerates of $LiNi_{0.975}Tl_{0.025}O_2$ are in the form of sphere.

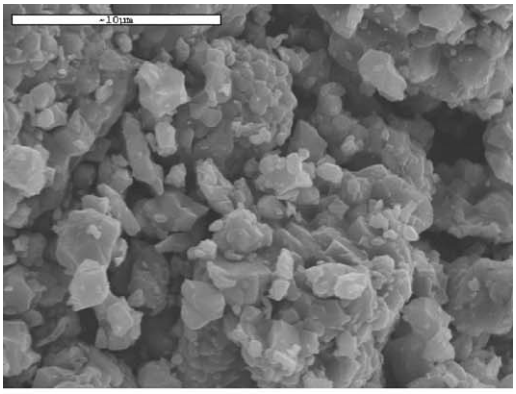

(a) $LiNi_{0.975}Ga_{0.025}O_2$

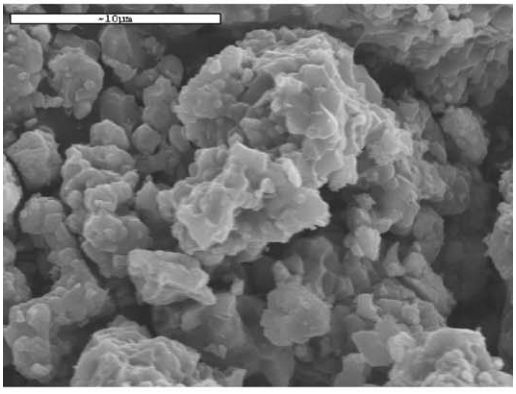

(b) $LiNi_{0.975}In_{0.025}O_2$

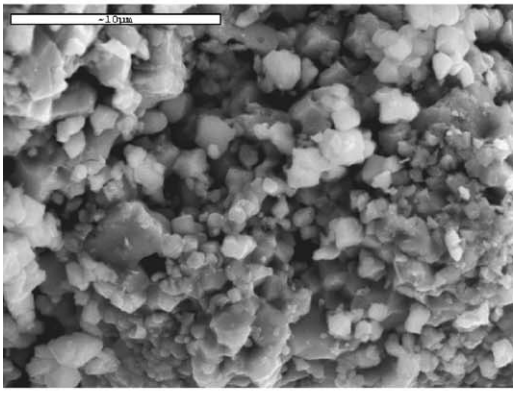

(c) $LiNi_{0.975}Tl_{0.025}O_2$

Fig. 3. SEM photographs of $LiNi_{0.975}M_{0.025}O_2$ (M = Ga, In and Tl) calcined at 750 °C for 36 h.

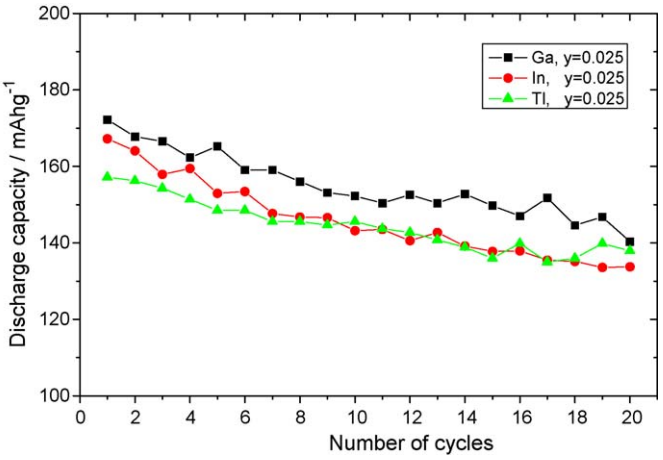

Fig. 4. Variations of the discharge capacity with the number of cycles for $LiNi_{0.975}M_{0.025}O_2$ (M = Ga, In and Tl) synthesized by the combustion method.

Fig. 4 shows variations of discharge capacity with number of cycles of $LiNi_{0.975}M_{0.025}O_2$ (M = Ga, In and Tl) synthesized by the combustion method. $LiNi_{0.975}Ga_{0.025}O_2$ has the largest first discharge capacity (172.2 mAh g^{-1}), followed by $LiNi_{0.975}In_{0.025}O_2$ (167.2 mAh g^{-1}) and $LiNi_{0.975}Tl_{0.025}O_2$ (157.2 mAh g^{-1}). $LiNi_{0.975}Tl_{0.025}O_2$ has the best cycling performance, followed by $LiNi_{0.975}Ga_{0.025}O_2$ and $LiNi_{0.975}In_{0.025}O_2$. They have the discharge capacity degradation rates of 1.07, 1.35 and 1.66 mAh g^{-1}/cycle, respectively.

Fig. 5 shows $-dQ/|dV|$ vs. voltage curve, where Q is charge or discharge capacity and V is voltage, at the first cycle and the second cycle for $LiNi_{0.975}Ga_{0.025}O_2$ synthesized by the combustion method. During charge and discharge, $LiNiO_2$ goes through several phase transitions such as phase transition from hexagonal (H1) to monoclinic (M), to hexagonal (H2) and to hexagonal (H3) or vice versa [35–37]. In addition, it is reported that at the phase transition from H2 to H3 contraction of lattice parameter *c*-axis occurs and then electrochemical properties become worse [34]. The sharp peak corresponds to a phase transition at which two phases co-exist and the broad peak corresponds to a phase transition at which one-phase changes continuously [31]. The oxidation peaks at 3.76, 4.03 and 4.24 V for the first cycle are considered to correspond to transitions from H1 to M, from M to H2 and from H2 to H3, respectively, and the peak for the continuous phase transition of M seems to be hidden within the peak for the transition from H1 to M. The reduction peaks at 4.14, 3.96, 3.70 and 3.62 V for the first cycle are considered to correspond to transitions from H3 to H2 and from H2 to M, continuous phase transition of M, and transition from M to H1, respectively. The oxidation peaks and the reduction peaks for the second cycle appear more clearly than those for the first cycle. This is considered to be because the unstable sites are destructed during de-intercalation and intercalation of the first cycle. The oxidation peak for the continuous phase transition of M appears broadly around 3.77 V.

Fig. 6 shows $-dQ/|dV|$ vs. voltage curve at the first cycle and the second cycle for $LiNi_{0.975}In_{0.025}O_2$ synthesized by the combustion method. The oxidation peaks at 3.71, 4.02 and 4.22 V for the first cycle are considered to correspond to

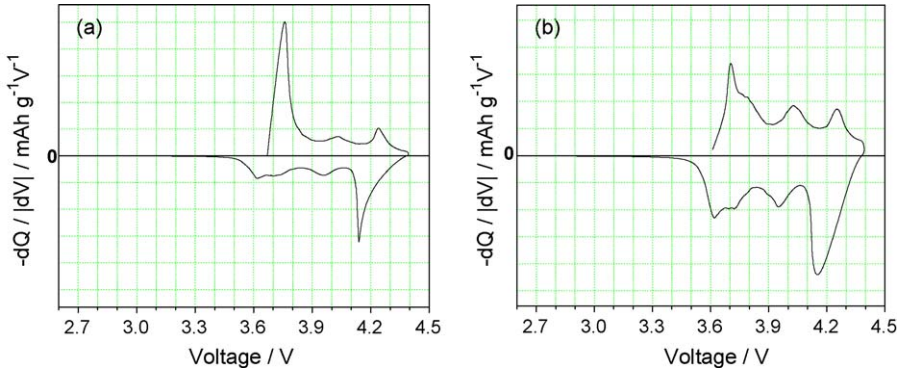

Fig. 5. $-dQ/|dV|$ vs. voltage curve for $LiNi_{0.975}Ga_{0.025}O_2$ synthesized by the combustion method; (a) the first cycle and (b) the second cycle.

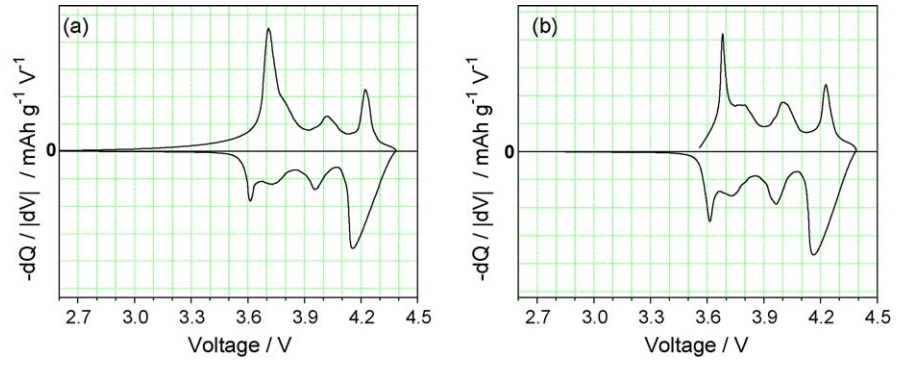

Fig. 6. $-dQ/|dV|$ vs. voltage curve for $LiNi_{0.975}In_{0.025}O_2$ synthesized by the combustion method; (a) the first cycle and (b) the second cycle.

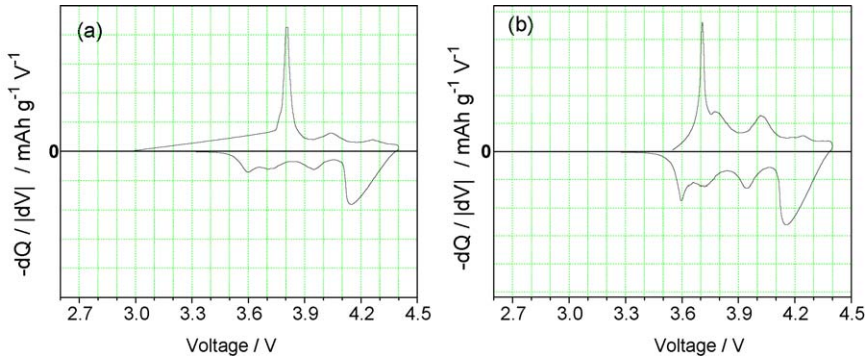

Fig. 7. $-\mathrm{d}Q/|\mathrm{d}V|$ vs. voltage curve for $LiNi_{0.975}Tl_{0.025}O_2$ synthesized by the combustion method; (a) the first cycle and (b) the second cycle.

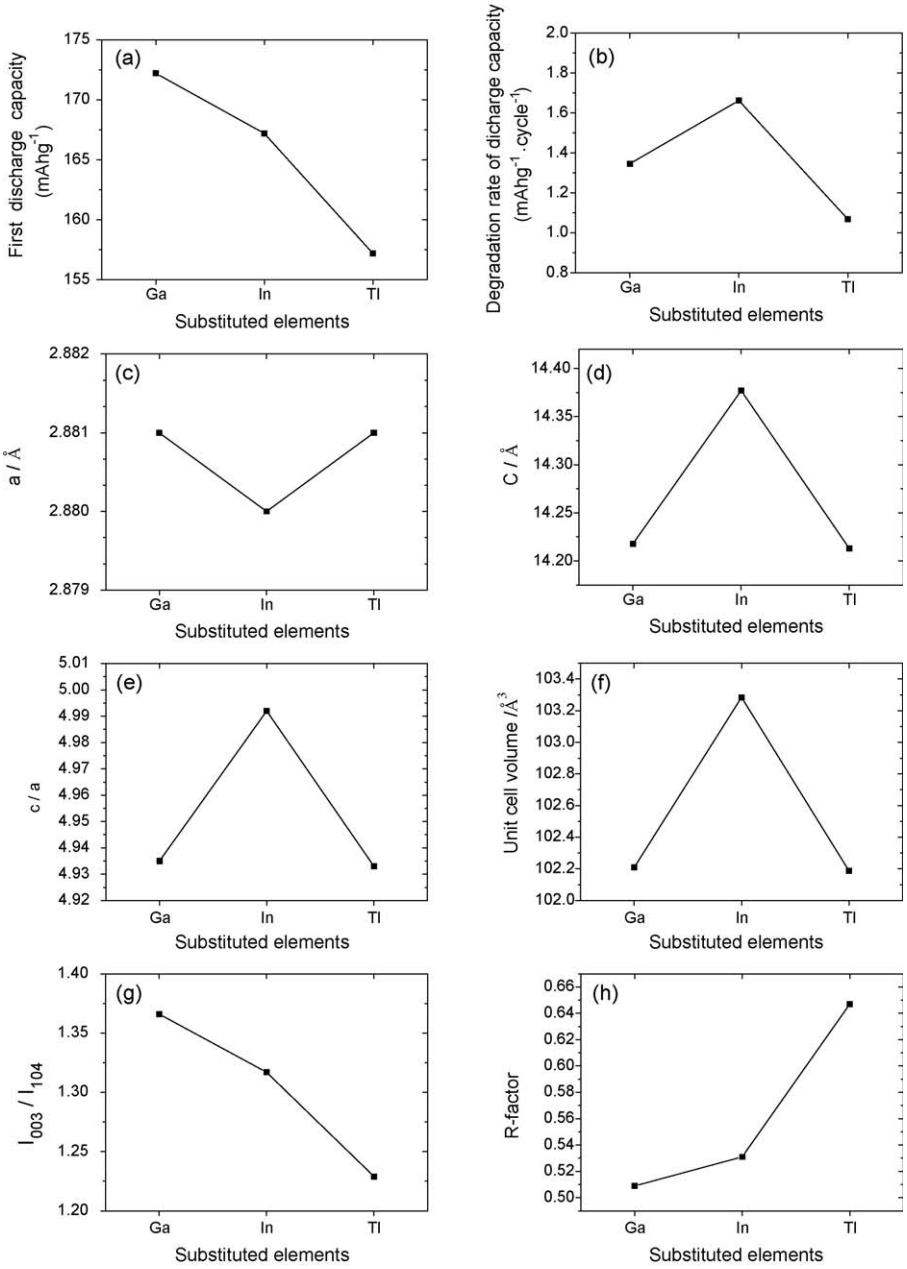

Fig. 8. Variations, with the substituted element, of (a) the first discharge capacity, (b) the degradation rate of discharge capacity, (c) the lattice parameter a, (d) the lattice parameter c, (e) c/a, (f) unit cell volume, (g) I_{003}/I_{104} and (h) R-factor for $LiNi_{0.975}M_{0.025}O_2$ (M = Ga, In and Tl) synthesized by the combustion method.

transitions similar to those for $LiNi_{0.975}Ga_{0.025}O_2$, respectively, and the peak for the continuous phase transition of M appears broadly around 3.78 V. The reduction peaks at 4.15, 3.96, 3.73 and 3.61 V for the first cycle are considered to correspond to transitions similar to those for $LiNi_{0.975}Ga_{0.025}O_2$, respectively. The oxidation peaks and the reduction peaks for the second cycle appear more clearly than those for the first cycle, as they are for $LiNi_{0.975}Ga_{0.025}O_2$. And the oxidation peak for the continuous phase transition of M appears broadly around 3.78 V.

Fig. 7 shows $-dQ/|dV|$ vs. voltage curve at the first cycle and the second cycle for $LiNi_{0.975}Tl_{0.025}O_2$ synthesized by the combustion method. The oxidation peaks at 3.80, 4.04 and 4.26 V for the first cycle are considered to correspond to transitions similar to those for $LiNi_{0.975}Ga_{0.025}O_2$ and $LiNi_{0.975}In_{0.025}O_2$, and the peak for the continuous phase transition of M does not appear. The reduction peaks at 4.15, 3.95, 3.71 and 3.60 V for the first cycle are considered to correspond to transitions similar to those for $LiNi_{0.975}Ga_{0.025}O_2$ and $LiNi_{0.975}In_{0.025}O_2$. The oxidation peaks and the reduction peaks for the second cycle appear more clearly than those for the first cycle, as they are for $LiNi_{0.975}Ga_{0.025}O_2$ and $LiNi_{0.975}In_{0.025}O_2$. And the oxidation peak for the continuous phase transition of M appears broadly around 3.78 V.

The oxidation and reduction peaks for $LiNi_{0.975}In_{0.025}O_2$ at the first cycle and the second cycle are sharper than those for $LiNi_{0.975}Ga_{0.025}O_2$ and $LiNi_{0.975}Tl_{0.025}O_2$. This suggests that the phase transition of $LiNi_{0.975}In_{0.025}O_2$ occurs at more distinct voltages than those of $LiNi_{0.975}Ga_{0.025}O_2$ and $LiNi_{0.975}Tl_{0.025}O_2$. It may be related to the better-defined crystal structure (crystallinity) of $LiNi_{0.975}In_{0.025}O_2$ than $LiNi_{0.975}Ga_{0.025}O_2$ and $LiNi_{0.975}Tl_{0.025}O_2$.

Fig. 8 shows the variations with the substituted element of (a) the first discharge capacity, (b) the degradation rate of discharge capacity, (c) the lattice parameter a, (d) the lattice parameter c, (e) c/a, (f) unit cell volume, (g) $I_{0\,0\,3}/I_{1\,0\,4}$ and (h) R-factor for $LiNi_{0.975}M_{0.025}O_2$ (M = Ga, In, and Tl) synthesized by the combustion method. The first discharge capacity and $I_{0\,0\,3}/I_{1\,0\,4}$ decrease and R-factor increases, as the substituted elements vary from Ga to In and then to Tl. The degradation rate of discharge capacity, the lattice parameter c, c/a and the unit cell volume have maximum values when the substituted element is In. The lattice parameter a has its minimum value when M = In. The variation of the first discharge capacity with the substituted element is similar to that of $I_{0\,0\,3}/I_{1\,0\,4}$. The large value of $I_{0\,0\,3}/I_{1\,0\,4}$ indicates low cation mixing. The decrease in $I_{0\,0\,3}/I_{1\,0\,4}$ from M = Ga through M = Tl is considered to be related to the decrease in the first discharge capacity from Ga through Tl substitution. The variation of the first discharge capacity with the substituted element is inversely proportional to that of R-factor. The sample with a small R-factor indicates low cation mixing. This sample has a large first discharge capacity. The variation of cation mixing with the substituted element is considered to be related to the behavior of the first discharge capacity with the substituted element. Although $LiNi_{0.975}In_{0.025}O_2$ has a small amount of impurity ($LiInO_2$), it has higher first discharge capacity than $LiNi_{0.975}Tl_{0.025}O_2$. Less cation mixing of $LiNi_{0.975}In_{0.025}O_2$, compared with $LiNi_{0.975}Tl_{0.025}O_2$, is considered to lead to this result. The degradation rate of discharge capacity is smallest when M = Tl.

4. Conclusions

$LiNi_{0.975}M_{0.025}O_2$ (M = Ga, In and Tl) synthesized by the combustion method (by preheating at 400 °C for 30 min in air and then calcining in an O_2 stream at 750 °C for 36 h) had the $R\bar{3}m$ structure, and $LiNi_{0.975}In_{0.025}O_2$ contained $LiInO_2$ phase as an impurity. Among these samples, $LaNi_{0.975}Ga_{0.025}O_2$ had the largest first discharge capacity (172.2 mAh g^{-1}) and relatively good cycling performance (discharge capacity 140.3 mAh g^{-1} at $n = 20$). For $LiNi_{0.975}M_{0.025}O_2$ (M = Ga, In and Tl), the first discharge capacity decreased with increase in the ionic radius of the substituted element. The variation of cation mixing with the substituted element (decrease in $I_{0\,0\,3}/I_{1\,0\,4}$ and increase in R-factor from M = Ga through M = Tl) is considered to be related to the behavior of the first discharge capacity with the substituted element.

Acknowledgement

This work was supported by grant No. R01-2003-000-10325-0 from the Basic Research Program of the Korea Science & Engineering Foundation.

References

[1] J.M. Tarascon, E. Wang, F.K. Shokoohi, W.R. McKinnon, S. Colson, J. Electrochem. Soc. 138 (1991) 2859.
[2] A.R. Armstrong, P.G. Bruce, Lett. Nat. 381 (1996) 499.
[3] M.Y. Song, D.S. Ahn, Solid State Ionics 112 (1998) 245.
[4] K. Ozawa, Solid State Ionics 69 (1994) 212.
[5] R. Alcátara, P. Lavela, J.L. Tirado, R. Stoyanova, E. Zhecheva, J. Solid State Chem. 134 (1997) 265.
[6] Z.S. Peng, C.R. Wan, C.Y. Jiang, J. Power Sources 72 (1998) 215.
[7] J.R. Dahn, U. von Sacken, C.A. Michal, Solid State Ionics 44 (1990) 87.
[8] J.R. Dahn, U. von Sacken, M.W. Juzkow, H. Al-Janaby, J. Electrochem. Soc. 138 (1991) 2207.
[9] A. Marini, V. Massarotti, V. Berbenni, D. Capsoni, R. Riccardi, E. Antolini, B. Passalacqua, Solid State Ionics 45 (1991) 143.
[10] W. Ebner, D. Fouchard, L. Xie, Solid State Ionics 69 (1994) 238.
[11] R. Kanno, H. Kubo, Y. Kawamoto, T. Kamiyama, F. Izumi, Y. Takeda, M. Takano, J. Solid State Chem. 110 (1994) 216.
[12] A. Hirano, R. Kanno, Y. Kawamoto, Y. Takeda, K. Yamaura, M. Takano, K. Ohyama, M. Ohashi, Y. Yamaguchi, Solid State Ionics 78 (1995) 123.
[13] A. Rougier, P. Gravereau, C. Delmas, J. Electrochem. Soc. 143 (1996) 1168.
[14] H. Arai, S. Okada, Y. Sakurai, J. Yamaki, Solid State Ionics 95 (1997) 275.
[15] Y. Nishida, K. Nakane, T. Stoh, J. Power Sources 68 (1997) 561.
[16] M. Broussely, J. Power Sources 81-82 (1990) 140.
[17] Y. Gao, M.V. Yakovleva, W.B. Ebner, Electrochem. Soc. 142 (1995) 702.
[18] D. Caurant, N. Baffier, B. Garcia, J.P. Pereira-Ramos, Solid State Ionics 91 (1996) 45.
[19] A. Rougier, I. Saadoune, P. Gravereau, P. Willmann, C. Delmas, Solid State Ionics 90 (1996) 83.
[20] S.H. Chang, S.G. Kang, S.W. Song, J.B. Yoon, J.H. Choy, Solid State Ionics 86–88 (1996) 171.
[21] Y. Gao, M.V. Yakovleva, W.B. Ebner, Electrochem. Solid State Lett. 1 (1998) 117.
[22] J. Kim, K. Amine, Electrochem. Commun. 3 (2001) 52.
[23] J. Kim, K. Amine, J. Power Sources 104 (2002) 33.

[24] M. Guilmard, A. Rougier, M. Grune, L. Croguennec, C. Delmas, J. Power Sources 115 (2003) 305.
[25] M. Guilmard, L. Croguennec, C. Delmas, J. Electrochem. Soc. 150 (10) (2003) A1287.
[26] M.Y. Song, R. Lee, I.H. Kwon, Solid State Ionics 156 (2003) 319.
[27] L. Zhang, X. Wang, H. Noguchi, M. Yoshio, K. Takada, T. Sasaki, Electrochim. Acta 49 (2004) 3305.
[28] T. Amriou, A. Sayede, B. Khelifa, C. Mathieu, H. Aourag, J. Power Sources 130 (2004) 213.
[29] E. Shinova, E. Zhecheva, R. Stoyanova, G.D. Bromiley, R. Alcántara, J.L. Tirado, J. Solid State Chem. 178 (2005) 2692.
[30] D. Tong, J. Cao, Q. Lai, A. Tang, K. Huang, Y. He, X. Ji, Mater. Chem. Phys. 100 (2–3) (2006) 217.
[31] S.R. Jain, K.C. Adiga, V. Pai Verneker, Combust. Flame 40 (1981) 71.
[32] Y. Zhang, G.C. Stangle, J. Mater. Res. 9 (1994) 1997.
[33] M.Y. Song, I.H. Kwon, H.U. Kim, S.B. Shim, D.R. Mumm, J. Appl. Electrochem. 36 (2006) 801.
[34] T. Ohzuku, A. Ueda, M. Nagayama, J. Electrochem. Soc. 140 (1993) 1862.
[35] H. Arai, S. Okada, H. Ohtsuka, M. Ichimura, J. Yamaki, Solid State Ionics 80 (1995) 261.
[36] W. Li, J.N. Reimers, J.R. Dahn, Solid State Ionics 67 (1993) 123.
[37] Q. Zhong, U. von Sacken, J. Power sources 54 (1995) 221.